Environmental Science and Pollution Research
https://doi.org/10.1007/s11356-017-1005-z

RESEARCH ARTICLE

Surface restructuring of red mud to produce $FeO_x(OH)_y$ sites and mesopores for the efficient complexation/adsorption of β-lactam antibiotics

Paula S. Pinto[1] · Giovani D. Lanza[1] · Mayra N. Souza[1] · José D. Ardisson[2] · Rochel M. Lago[1]

Received: 22 September 2017 / Accepted: 10 December 2017

Abstract
In this work, iron oxide in the red mud (RM) waste was restructured to produce mesopores with surface [$FeO_x(OH)_y$] sites for the efficient complexation/adsorption of β-lactam antibiotics. Red mud composed mainly by hematite was restructured by an acid/base process followed by a thermal treatment at 150–450 °C (MRM150, MRM200, MRM300, and MRM450) and fully characterized by Mössbauer, XRD, FTIR, BET, SEM, CHN, and thermogravimetric analyses. The characterization data showed a highly dispersed Fe^{3+} oxyhydroxy phase, which was thermally dehydrated to a mesoporous α-Fe_2O_3 with surface areas in the range of 141–206 $m^2\ g^{-1}$. These materials showed high efficiencies (21–29 mg g^{-1}) for the adsorption of β-lactam antibiotics, amoxicillin, cephalexin, and ceftriaxone, and the data was better fitted by the Langmuir model isotherm ($R^2 = 0.9993$) with monolayer adsorption capacity of ca. 39 mg g^{-1} for amoxicillin. Experiments such as competitive adsorption in the presence of phosphate and H_2O_2 decomposition suggested that the β-lactamic antibiotics might be interacting with surface [$FeO_x(OH)_y$] species by a complexation process. Moreover, the OH/Fe ratio, BET surface area and porosity indicated that this complexation is occurring especially on $[FeO_x(OH)_y]_{surf}$ sites contained in the mesopore space.

Keywords Beta-lactam antibiotics · Red mud · Adsorption · Amoxicillin · Iron oxide · Complexation · Iron oxyhydroxy

Introduction

Red mud (RM) is a hazardous alkaline waste from the Bayer process with an estimated production of ca. 70 billion t $year^{-1}$ containing different metal oxides, e.g., Si, Al, Fe, and Ti (Sutar et al. 2014). The high concentration of iron oxides in RM (ca. 30–50%) led to the investigation of different technological applications of this waste, such as coagulant (Ni et al. 2015), bio-oil upgrade (Karimi et al. 2014, Karimi et al. 2012), wastewater treatment by heterogeneous Fenton (Costa et al. 2010), a combined process to recover iron and produce fuel from bio-oil waste fractions (Mendonça et al. 2016), production of carbon nanotubes/nanofibers (Oliveira et al. 2010, Oliveira et al. 2011, Teixeira et al. 2012), and storage and transport of offshore gas as carbon (Teixeira et al. 2014). The use of red mud as adsorbent has also been extensively investigated due to its potential to remove different aquatic pollutants such as metal ions, e.g., Ni(II) and As(V) (Castaldi et al. 2010, Smičiklas et al. 2014); textile dyes (Hajjaji et al. 2016, Tor and Cengeloglu 2006); phenolic compounds (Tor et al. 2006, Tor et al. 2009); and phosphate (Ye et al. 2015, Yue et al. 2010). Several treatments have been suggested in literature to increase the adsorption properties in red mud, like acid treatment, e.g., HCl, H_2SO_4, and HNO_3, for the adsorption of fluoride and heavy metals (Apak et al. 1998, Liang et al. 2014, Santona et al. 2006); heat treatments to adsorb arsenic (Altundoğan et al. 2002); and mixing the red mud with calcium- and magnesium-ion solutions for phosphate adsorption (Ye et al. 2016). Nevertheless,

Responsible editor: Guilherme L. Dotto

Electronic supplementary material The online version of this article (https://doi.org/10.1007/s11356-017-1005-z) contains supplementary material, which is available to authorized users.

✉ Rochel M. Lago
rochel@ufmg.br

[1] Departamento de Química, Universidade Federal de Minas Gerais (UFMG), Belo Horizonte, MG 31270-901, Brazil

[2] Laboratório de Física Aplicada, Centro de Desenvolvimento da Tecnologia Nuclear (CDTN/CNEN), Belo Horizonte, MG 31270-901, Brazil

Published online: 20 December 2017

no study was found in literature about the creation of specific sites based on Fe^{3+} for the adsorption of β-lactamic antibiotic molecules.

The presence of antibiotics in water may cause adverse effects such as chronic toxicity inducing the resistance of pathogenic microorganisms (Ali et al. 2009, Dong et al. 2016, Pezoti et al. 2016, Tian et al. 2016). Since conventional treatments are not efficient to remove these hazardous contaminants from wastewaters, antibiotics have become a relevant environmental issue (Liu et al. 2016b).

The class of β-lactam is the most important group of antibiotics corresponding to 50–70% of total antibiotics consumed in the world (Rahimi et al. 2015). There are several proposed methods to remove β-lactam antibiotics from wastewaters, e.g., Fenton (Pourakbar et al. 2016), photocatalysis (Weng et al. 2014), ozonolysis (Marcelino et al. 2017), electrochemical oxidation (Liu et al. 2015b), reverse osmosis (Liu et al. 2015a), and biodegradation (Dong et al. 2016). Adsorptive methods have been extensively studied showing good efficiencies and technical simplicity (Ali 2012, 2014, Ali and Gupta 2007, Chayid and Ahmed 2015). Some of the materials used as adsorbents for antibiotic contaminants are activated carbons (Liu et al. 2016a, Pouretedal and Sadegh 2014), clay (Saitoh and Shibayama 2016), molecularly imprinted polymer (Yin et al. 2010), carbon nanotubes (Fazelirad et al. 2015), ion-exchange resin (Wang et al. 2017), and iron nanoparticles (Ghauch et al. 2009). A recent work showed that supported iron oxide, i.e., Fe_2O_3/Al_2O_3, prepared in specific conditions showed surprisingly high efficiencies for the adsorption of β-lactam antibiotics (Pinto et al. 2016). The adsorption results were discussed in terms of $FeO_x(OH)_y$ surface species capable of complexing the antibiotic molecules.

In this work, the surface of the iron oxide present in the RM waste was chemically restructured in order to produce mesopore spaces to allow diffusion of large β-lactam antibiotic molecules and their adsorption by complexation on Fe^{3+} surface sites.

Experimental

Synthesis of materials

RM (Alcan, Brazil) was extensively washed with distilled water to a neutral pH and dried. The restructuring of iron oxide(III) in the red mud (10 g) was carried out by a treatment with $HCl_{conc.}$ (120 mL, Vetec) 80–90 °C 1 h^{-1} for a partial dissolution followed by precipitation with NH_4OH (Vetec) added dropwise to reach pH 9. The obtained solid, named as modified red mud (MRM), was treated at different temperatures (150, 200, 300, and 450 °C) for 3 h in a tubular furnace in air atmosphere producing four materials that have been named as MRM150, MRM200, MRM300, and MRM450, respectively.

Characterization

The physicochemical properties of the adsorbents were characterized by Mössbauer spectroscopy (^{57}Co source in a Rh matrix using α-Fe as reference spectrum at room temperature), powder XRD (Shimadzu XRD-7000 Cu radiation), SEM (FEI Quanta FEG 3D FEI microscope), infrared spectroscopy (PerkinElmer FTIR GX, KBr pellet), superficial-area BET (Quantachrome Autosorb-1 using N_2 at 77 K), thermogravimetric (TG)/derivative thermogravimetric (DTG) (TG DTG Shimatzu-60H performed in N_2 atmosphere, with a heating rate of 10 °C min^{-1} up to 700 °C), and elemental analyses (PerkinElmer CHN-PE-2400).

Adsorption experiments

The adsorbents were tested (20 mg) for the adsorption of β-lactam antibiotics (20 mL, 100 ppm, pH ~ 5–6) at 25 ± 2 °C. The antibiotic removal was monitored by the maximum absorptions at 272, 260, and 262 nm on UV/Vis (Shimadzu UV-2550), for amoxicillin (AMX), cephalexin (CEP), and ceftriaxone (CEF), respectively. The adsorption isotherm was obtained using 20 mg of MRM150 in contact with different amoxicillin concentrations (25, 50, 75, 100, 150, 200, 250, 300, 350, and 400 mg L^{-1}, pH ~ 5–6) during 24 h, and the experimental data were adjusted using the Langmuir and Freundlich isotherm models.

Competitive adsorption experiment was carried out using MRM150 (20 mg) in contact with a solution (20 mL) containing phosphate (25 mg L^{-1}) and amoxicillin (200 mg L^{-1}).

The H_2O_2 decomposition experiments were carried out as described previously (Pinto et al. 2016).

Results and discussion

Characterization

The chemical composition of the original RM used in this work was ca. 49 wt% Fe (as Fe_2O_3), 12 wt% Al (as Al_2O_3), 2 wt% TiO_2, 1 wt% Ca (as CaO), and silica. The RM sample was treated with HCl and NH_4OH followed by thermal treatment at 150, 200, 300, and 400 °C.

The Mössbauer spectra (Fig. 1) showed for the original RM precursor two iron phases, one related to hematite Fe_2O_3 (53%) and another to a highly dispersed/nanostructured phase containing superparamagnetic Fe^{3+} (47% spectral area).

The obtained results for the treated samples suggested that the restructuring process strongly attacked the hematite phase converting 100% to a superparamagnetic Fe^{3+}phase, even

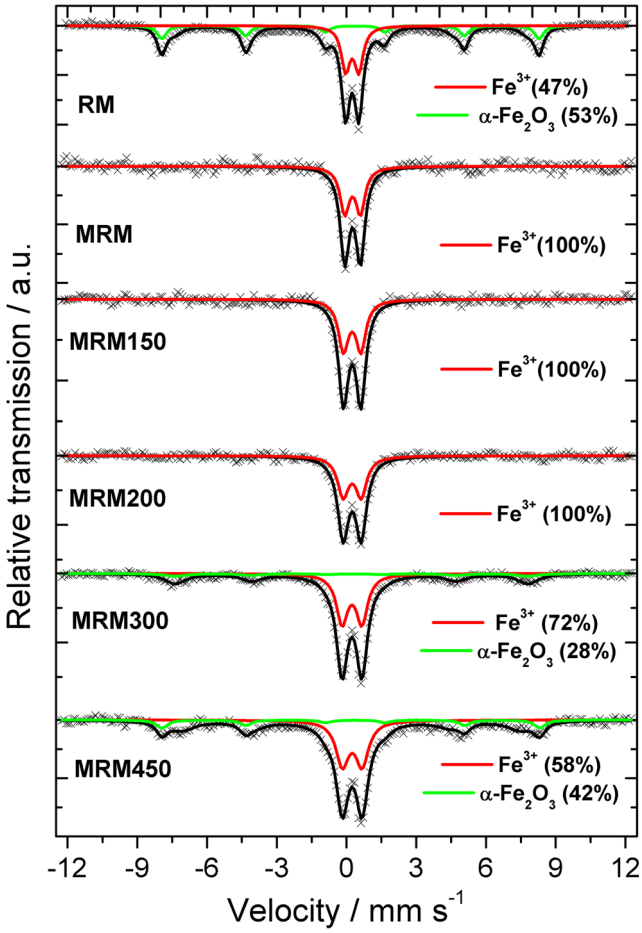

Fig. 1 Mössbauer spectra for RM before and after chemical restructuring and thermal treatment at 150, 200, 300, and 450 °C

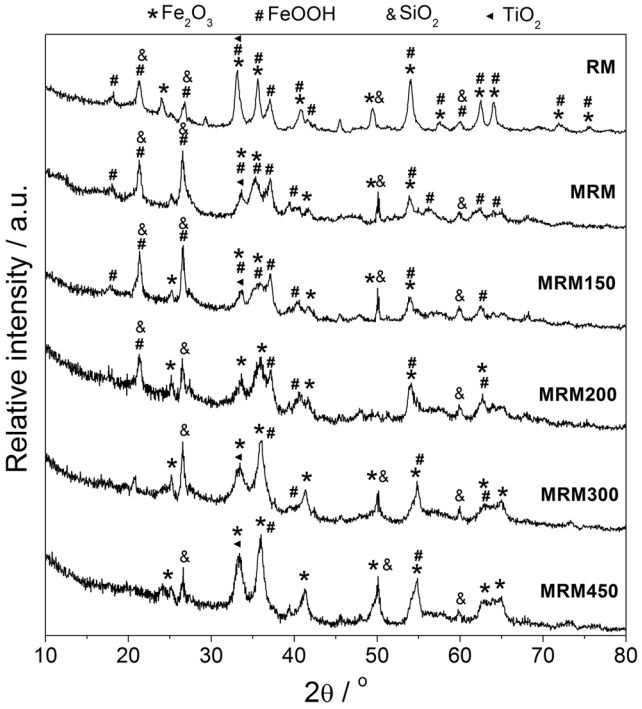

Fig. 2 XRD analyses for RM before and after chemical restructuring and thermal treatment at 150, 200, 300, and 450 °C

after thermal treatment at 150 and 200 °C, i.e., MRM, MRM150, and MRM200. When the sample was treated at higher temperatures, the superparamagnetic phase was gradually converted to hematite. At 300 and 450 °C, a well-organized hematite phase is formed with 28 and 42% spectral areas, respectively.

XRD analysis of the original RM (Fig. 2) indicated the presence of hematite (α-Fe_2O_3) with well-defined peaks at 33°, 36°, 63°, and 64° (PDF 33–664) which agreed with the Mössbauer data. Moreover, the XRD data also indicated the presence of alumina (Al_2O_3), titania (TiO_2), and silica (SiO_2) phases.

After chemical treatment, i.e., sample MRM, the hematite peaks became less intense and broad suggesting a loss of crystallinity. Upon treatment at 150 and 200 °C, no significant change in the XRD profile was observed. On the other hand, a significant crystallization took place in the treatment at 300 and 450 °C to form the α-Fe_2O_3 phase.

Crystallite average size of α-Fe_2O_3 estimated by the Scherrer equation showed values of approximately 33 nm for the original RM. When MRM was treated at 150, 200, 300, and 450 °C, the crystallite size varied from 10 nm for the MRM150 to 12, 13, and 15 nm, respectively.

It is interesting to consider that Mössbauer data suggested that most of the Fe^{3+} phases are present as amorphous Fe oxide and hydroxide, a highly dispersed phase which cannot be observed by XRD.

The SEM images (Fig. 3) showed in general no significant difference in the texture and morphology of RM and MRM samples. However, upon treatment at 150 and 200 °C, SEM images suggested the formation of some amorphous porous structure (Fig. 3).

It is also interesting to observe by EDS mapping measurements (see Electronic Supplementary Material—Fig. S1) that the Fe is completely disperse throughout the RM sample. After the restructuring process, no significant difference was observed in the Fe distribution on the sample surfaces.

The infrared spectrum of RM showed broad bands assigned to O–H stretch vibrations from iron, aluminum, and silica oxide/hydroxide and H–O–H adsorbed molecules, between 3550 and 3234 cm^{-1} (Fig. 4). It is interesting to observe that the relative intensities of these O–H bands decrease with respect to the related Si–O and Fe–O bands. The vibrations of Si–O and Si–O–Si bonds were observed at 3334, 1115, 994, and 617 cm^{-1} (Miller and Wilkins 1952). After chemical and thermal treatments, the disappearance of the band at 994 cm^{-1} indicated a partial dissolution of Si-O species (Liang et al. 2014). A typical Fe_2O_3 band at 472 cm^{-1} was observed in infrared spectrum for all samples (Cornell and Schwertmann 2004).

BET analysis showed a surface area of 38 $m^2\ g^{-1}$ for the RM and no significant pore volume (Fig. 5). The surface

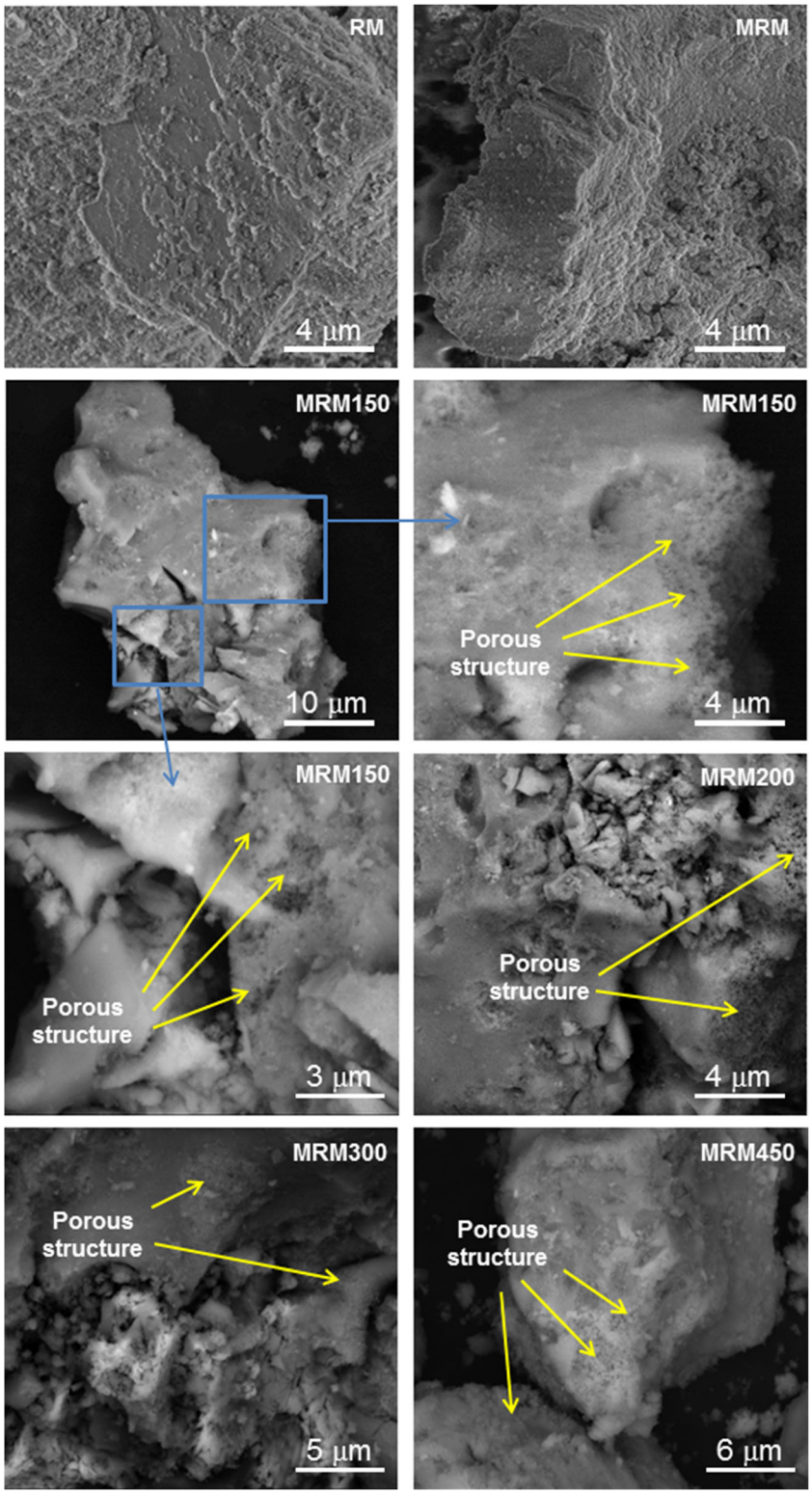

Fig. 3 SEM images of RM, MRM, MRM150, MRM200, MRM300, and MRM450

restructuring with subsequent thermal treatment at 150 °C (MRM150) increased the surface area to ca. 200 $m^2\ g^{-1}$. This increase can be related to the partial dissolution and conversion of the hematite phase especially into meso- and macroporous $Fe(OH)_3$/FeOOH phases.

The thermal treatment at 200 °C (MRM200) produced a slight increase in the surface area to 206 $m^2\ g^{-1}$, due to the porosity created by water loss of $Fe(OH)_3$/FeOOH phase in the sample. As the temperature was increased to 300 and 450 °C, a decrease on the BET surface to 174 and 141 $m^2\ g^{-1}$

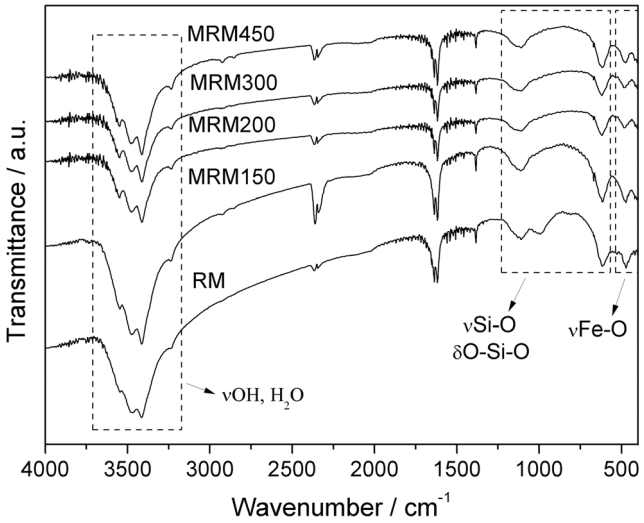

Fig. 4 IR spectra for the RM before and after chemical restructuring and thermal treatment at 150, 200, 300, and 450 °C

for MRM300 and MRM450, respectively, was observed, probably due to dehydration and sinterization process that typically takes place with FeOOH phases (Zboril et al. 2002).

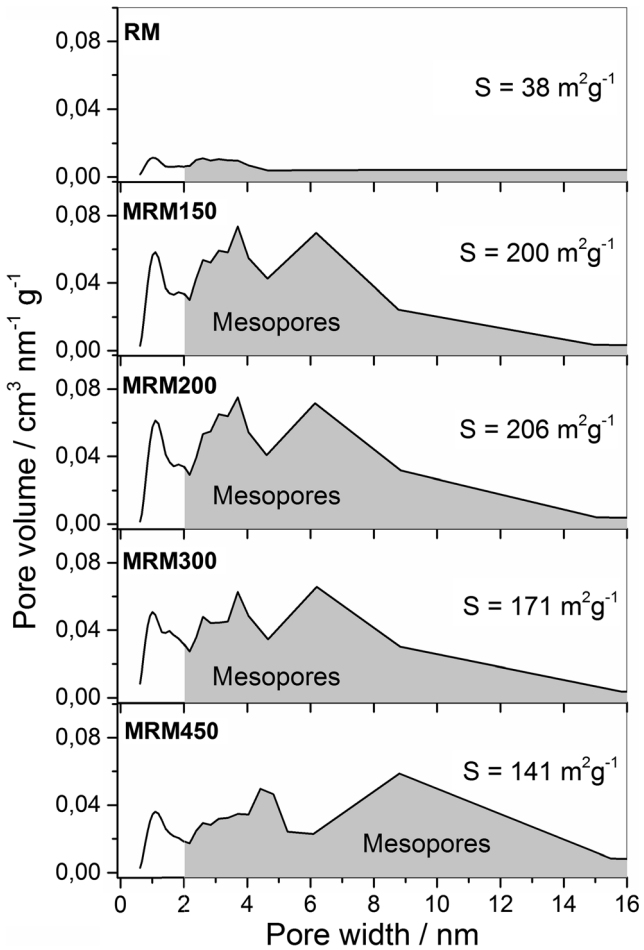

Fig. 5 BET surface area and porosity for the RM before and after chemical restructring and thermal treatment at 150, 200, 300, and 450 °C

TG analysis/DTA of the RM (Fig. 6) showed three important endothermic losses. The first weight loss at temperatures lower than 100 °C is related to adsorbed water. The second loss centered at 260 °C is likely related to the dehydroxylation of Fe-OH species, such as FeOOH (Liu et al. 2016c). At higher temperature, 330 °C, the weight loss is probably related to the dihydroxylation of Al-OH and Si-OH species (Liu et al. 2016c, Pascual et al. 2009).

It is interesting to observe that as the thermal treatment increased, the two weight losses due to dehydroxylation at 260 and 330 °C gradually decreased. TG/DTA analysis of the sample MRM200 showed that the loss at 260 °C completely disappeared suggesting that treatment at 200 °C converted all Fe-OH species onto Fe_2O_3. Also, the evaluation of the MRM300 and MRM450 thermograms indicated that these treatments led to the complete dehydroxylation of the Al and Si hydroxyl species.

The hydrogen contents were obtained by elemental analysis, i.e., 0.72, 1.83, 1.34, 1.23, 0.88, and 0.25 wt%, for the samples RM, MRM, MRM150, MRM200, MRM300, and MRM450, respectively. Considering the TG weight losses and H percentage, it was possible to estimate the $FeO_x(OH)_y$ composition for all the samples. The MRM showed the approximate composition of $FeO_{1.38}(OH)_{0.25}$ which after thermal treatment at 150 °C (MRM150) turned to a composition of ca. $FeO_{1.41}(OH)_{0.19}$. After 200 and 300 °C thermal treatments, similar compositions were obtained, i.e., $FeO_{1.46}(OH)_{0.07}$ and $FeO_{1.47}(OH)_{0.06}$, respectively. At 450 °C, the OH content further decreased to an estimated composition of $FeO_{1.49}(OH)_{0.02}$ which is very close to the composition Fe_2O_3. These results clearly indicate a continuous dehydroxylation process during the conversion of the Fe oxyhydroxy phase to the oxide Fe_2O_3.

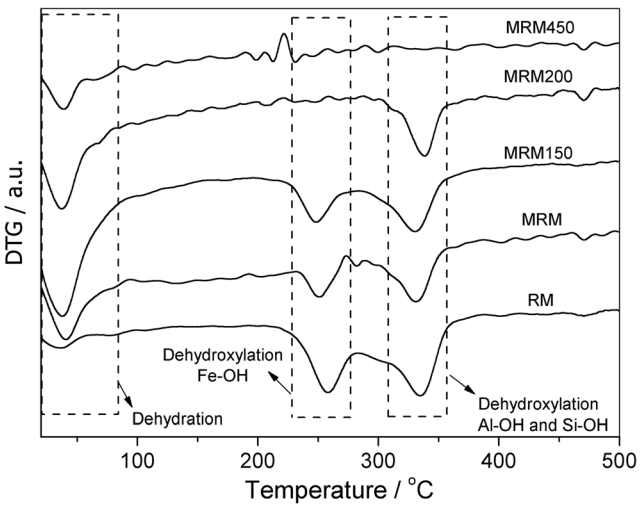

Fig. 6 DTG analyses of the samples treated at different temperatures

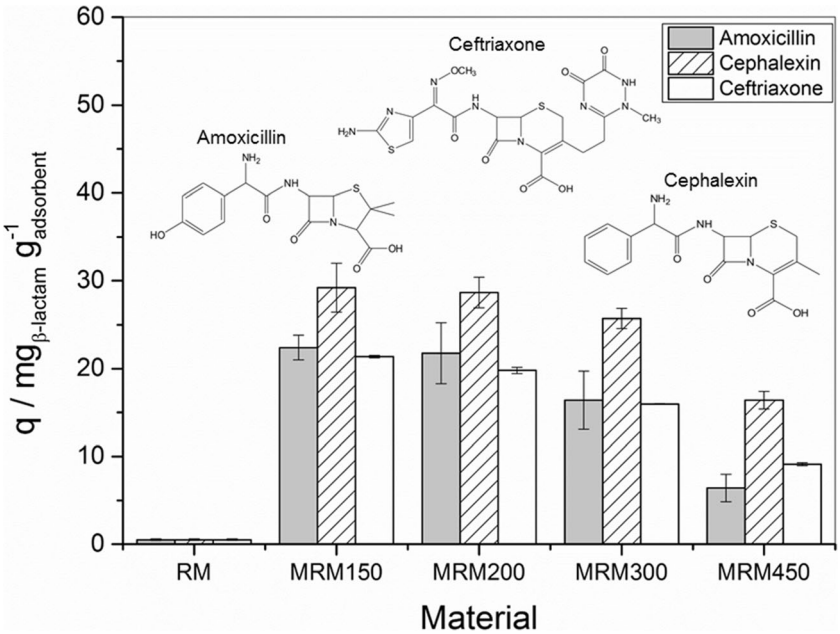

Fig. 7 Amoxicillin, cephalexin and ceftriaxone adsorption on RM and MRM treated at different temperatures

Antibiotic adsorption

The adsorption capacities for the prepared materials were obtained for three different β-lactam antibiotic adsorption (amoxicillin, cephalexin, and ceftriaxone), and the results are shown in Fig. 7.

The RM showed no significant antibiotic adsorption for all β-lactam antibiotics. After restructuring and thermal treatment at 150 °C, the MRM150 sample adsorbed significant amounts of the antibiotics, ca. 22, 29, and 21 mg g^{-1} of amoxicillin, cephalexin, and ceftriaxone, respectively. As the thermal treatment increased to 200 and 300 °C, a slight decrease on adsorption was verified, reaching values of 21 and 16 mg g^{-1} for amoxicillin, 28 and 25 mg g^{-1} for cephalexin, and 20 and 16 mg g^{-1} for ceftriaxone, respectively. On the other hand, treatment at 450 °C led to a more significant decrease of the adsorption capacity, i.e., 6, 16, and 9 mg g^{-1} for amoxicillin, cephalexin, and ceftriaxone, respectively. The MRM sample was also tested in adsorption experiments, but atomic absorption measurements in the aqueous phase showed significant Fe^{3+} leaching from the material.

Based on the literature, classical isotherm models, such as Langmuir and Freündlich; statistical physics models such as Hill (Sellaoui et al. 2017b); and phenomenological model (Sellaoui et al. 2017a) have been used to better understand the experimental data obtained from pharmaceutical adsorption. In this work, a preliminary modeling was carried out using the classical models which have been used to fit a wide range of experimental data (Fazelirad et al. 2015, Liu et al. 2016a, Moussavi et al. 2013).

Therefore, the better results were obtained for the Langmuir model ($R^2 = 0.9993$) compared to the Freündlich model ($R^2 = 0.9360$) (see Electronic Supplementary Material—Fig. S2). The maximum monolayer adsorption capacity obtained from the Langmuir model was 43 mg g^{-1}, which is close to the experimental data, ca. 39 mg g^{-1}. More detailed experimental data is necessary to investigate the use of more complex models in order to understand the adsorption process.

To better understand the role of the iron species, a competitive adsorption experiment was carried out in the presence of phosphate. The obtained result showed that the AMX adsorption decreased from 41 to 7 mg AMX g^{-1} in the presence of 25 mg phosphate L^{-1}. Although the reason for this effect is not clear, it is known that phosphates can complex surface Fe^{3+} species and hinder the interaction with other species in aqueous medium (Pinto et al. 2016, Qin et al. 2014). Therefore, this result suggested that the AMX adsorption might be related to a Fe^{3+}-AMX-specific interaction/complexation process.

The effect of AMX on the inhibition of the H_2O_2 decomposition process was also investigated, and the results are shown in Fig. 8. It can be observed that the material MRM150 is catalytically active to decompose hydrogen peroxide. This activity should be related to the interaction of H_2O_2 molecules in the coordination sphere of surface Fe^{3+} species (Pereira et al. 2012):

$$Fe^{3+} + H_2O_2 \rightarrow [Fe(OOH)]^{2+} + H^+.$$

$$[Fe(OOH)]^{2+} \rightarrow Fe^{2+} + {}^{\cdot}OOH.$$

$$Fe^{3+} + {}^{\cdot}OOH \rightarrow Fe^{2+} + O_2 + H^+$$

On the other hand, the H_2O_2 decomposed in the presence of the antibiotic and showed a strong decrease in peroxide decomposition. This inhibition effect is likely related to the complexation of AMX molecules on these surface Fe^{3+} sites which hindered the H_2O_2 access to the metal coordination sphere (Pinto et al. 2016).

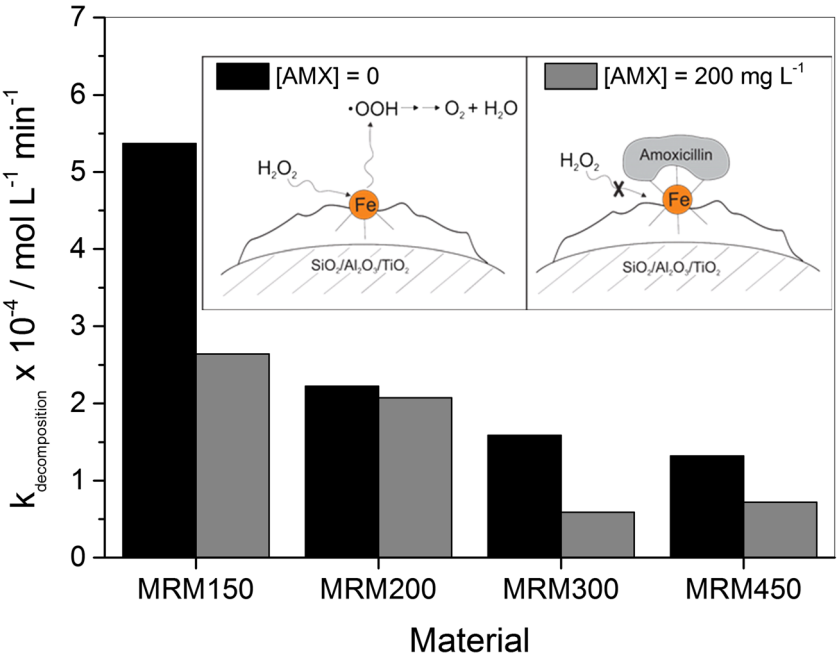

Fig. 8 H_2O_2 decomposition in the absence ([AMX] = 0) and presence ([AMX] = 200 mg L^{-1}) of AMX

In order to compare different adsorbents and the interaction of AMX with their surfaces, the adsorptions per square meter were calculated based on the isotherms and are compared in Fig. 9. The adsorbents MRM150, MRM200, and MRM300 showed similar values of ca. 0.2 mg AMX m^{-2} whereas the sample MRM450 showed a lower value, i.e., 0.1 mg AMX m^{-2}, indicating that the adsorption process is dependent not only on the surface area but also on the nature of the adsorption sites. It is also interesting to compare the normalized adsorption of the MRM adsorbents with other carbon-based adsorbents (Fig. 9) which have a greater surface area than the modified red muds, i.e., 1065 m^2 g^{-1} for KAC (microwave-prepared activated carbon (Chayid and Ahmed 2015)), 671 m^2 g^{-1} for MNPs_PAC (magnetic Fe_3O_4@C nanoparticles (Kakavandi et al. 2014)), 1055 m^2 g^{-1} for OP (activated carbon modified by oxidation (Mansouri et al. 2015)), 660 m^2 g^{-1} for TNC (templated nanoporous carbon (Barrera et al. 2014)), and 935 m^2 g^{-1} for AC (commercial activated carbon (Barrera et al. 2014)).

It can be observed that the specific adsorption capacity of MRM150 is comparable to the best materials in the literature. Only a synthetic material also based on Fe^{3+} supported on Al_2O_3 showed higher adsorption capacity (iron oxide supported on alumina, 107 m^2 g^{-1} (Pinto et al. 2016)).

Figure 10 shows the adsorption capacities with the surface area and OH/Fe mole ratios for the different MRM materials.

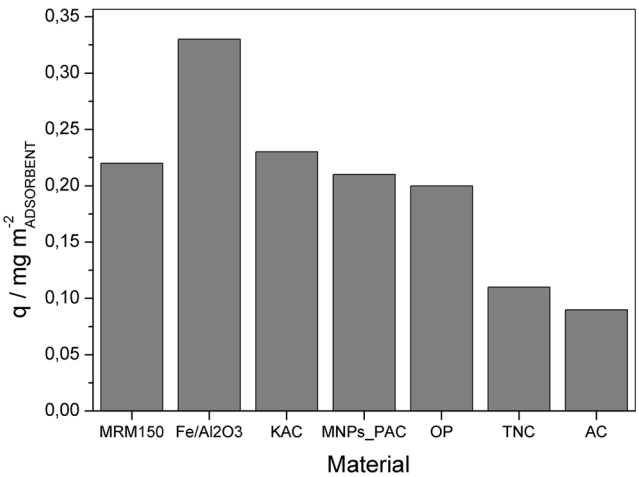

Fig. 9 Adsorption capacities (q) in milligram per square meter of different materials

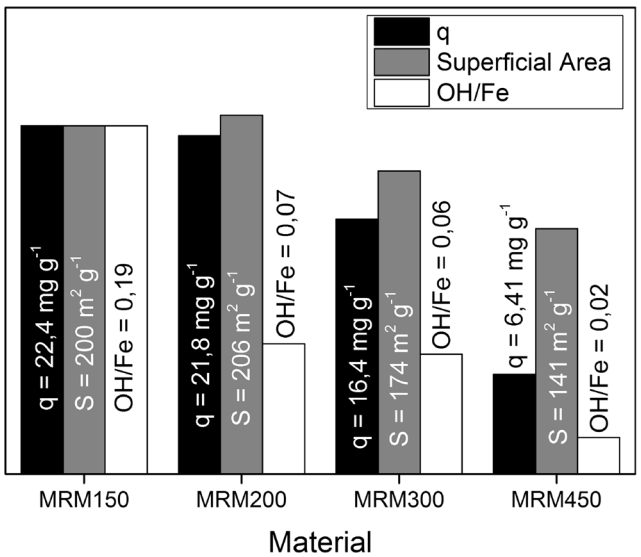

Fig. 10 Amoxicillin adsorption, OH/Fe ratio, and surface area for the different MRM-modified adsorbents

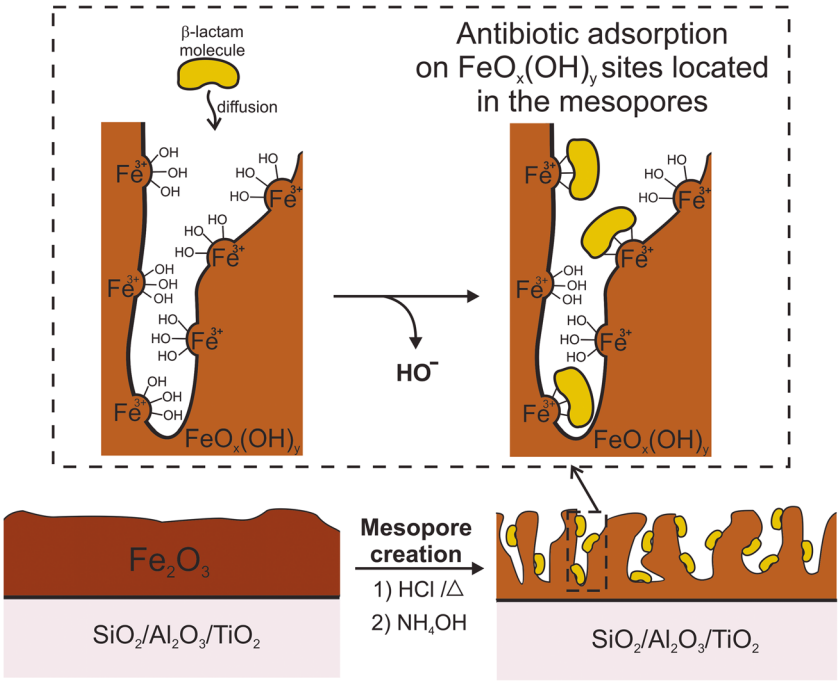

Fig. 11 Schematic representation of the restructuring of the Fe oxide in RM to produce mesopores for the adsorption/complexation of amoxicillin

It can be observed that the OH/Fe ratio for the MRM200 sample strongly decreased but the adsorption did not decrease significantly suggesting in this case that the surface is more important to determine the adsorption capacity. For the sample MRM300, the small decrease on the surface area appears to be responsible for the decrease observed on the AMX adsorption. On the other hand, the strong decrease on the AMX adsorption for the MRM450 sample seems to be more related to the decrease in OH/Fe (Fig. 10).

Although more detailed experiments are necessary to understand these data, one can consider that the treatment of red mud led to an increase of the surface area and the creation of mesopores containing Fe surface sites available for the complexation of amoxicillin molecules. The mesopores are important for the adsorption of the relatively large amoxicillin molecules (16 Å × 19 Å × 7 Å) (Boles et al. 1978). Also, on the surface of the mesopores, the formation of $FeO_x(OH)_y$ sites containing labile OH ligands seems to be important for the β-lactam antibiotic adsorption by complexation (Pinto et al. 2016).

Based on these results, a simplified schematic representation of the AMX adsorption process on the restructured RM material is shown in Fig. 11.

Conclusions

Red mud waste can be modified by simple acid/base and thermal treatments to produce a mesoporous Fe oxide phase containing surface $FeO_x(OH)_y$ sites efficiently for the adsorption of the hazardous β-lactamic antibiotics. These results demonstrate the possibility to modify different Fe-rich wastes to produce efficient adsorbents of β-lactam antibiotics and other large pharmaceutical hazardous molecules.

Funding information The authors gratefully acknowledge the financial support of the MIDAS INCT, CNPq, CAPES, FAPEMIG, and UFMG Microscopy Center.

References

Ali I (2012) New generation adsorbents for water treatment. Chem Rev 112(10):5073–5091. https://doi.org/10.1021/cr300133d

Ali I (2014) Water treatment by adsorption columns: evaluation at ground level. Sep Purif Rev 43(3):175–205. https://doi.org/10.1080/15422119.2012.748671

Ali I, Gupta VK (2007) Advances in water treatment by adsorption technology. Nat Protoc 1(6):2661–2667. https://doi.org/10.1038/nprot.2006.370

Ali I, Aboul-Enein HY, Gupta VK (2009) Nanochromatography and nanocapillary electrophoresis: pharmaceutical and environmental analyses. Wiley & Sons, Hoboken. https://doi.org/10.1002/9780470434925

Altundoğan HS, Altundoğan S, Tümen F, Bildik M (2002) Arsenic adsorption from aqueous solutions by activated red mud. Waste Manag 22(3):357–363. https://doi.org/10.1016/S0956-053X(01)00041-1

Apak R, Tütem E, Hügül M, Hizal J (1998) Heavy metal cation retention by unconventional sorbents (red muds and fly ashes). Water Res 32(2):430–440. https://doi.org/10.1016/S0043-1354(97)00204-2

Barrera D, Villarroel-Rocha J, Tara J, Basaldella E, Sapag K (2014) Synthesis and textural characterization of a templated nanoporous carbon from MCM-22 zeolite and its use as adsorbent of amoxicillin and ethinylestradiol. Adsorption 20(8):967–976. https://doi.org/10.1007/s10450-014-9640-x

Boles MO, Girven RJ, Gane PAC (1978) The structure of amoxycillin trihydrate and a comparison with the structures of ampicillin. Acta Crystallographica Section B 34(2):461–466. https://doi.org/10.1107/S0567740878003350

Castaldi P, Silvetti M, Enzo S, Melis P (2010) Study of sorption processes and FT-IR analysis of arsenate sorbed onto red muds (a bauxite ore processing waste). J Hazard Mater 175(1-3):172–178. https://doi.org/10.1016/j.jhazmat.2009.09.145

Chayid MA, Ahmed MJ (2015) Amoxicillin adsorption on microwave prepared activated carbon from Arundo donax Linn: isotherms, kinetics, and thermodynamics studies. J Environ Chem Eng 3(3): 1592–1601. https://doi.org/10.1016/j.jece.2015.05.021

Cornell RM, Schwertmann U (2004) Characterization, the iron oxides. Wiley-VCH Verlag GmbH & Co. KGaA, Weinheim, pp 139–183

Costa RCC, Moura FCC, Oliveira PEF, Magalhães F, Ardisson JD, Lago RM (2010) Controlled reduction of red mud waste to produce active systems for environmental applications: heterogeneous Fenton reaction and reduction of Cr(VI). Chemosphere 78(9):1116–1120. https://doi.org/10.1016/j.chemosphere.2009.12.032

Dong H, Yuan X, Wang W, Qiang Z (2016) Occurrence and removal of antibiotics in ecological and conventional wastewater treatment processes: a field study. J Environ Manag 178:11–19. https://doi.org/10.1016/j.jenvman.2016.04.037

Fazelirad H, Ranjbar M, Taher MA, Sargazi G (2015) Preparation of magnetic multi-walled carbon nanotubes for an efficient adsorption and spectrophotometric determination of amoxicillin. J Ind Eng Chem 21:889–892. https://doi.org/10.1016/j.jiec.2014.04.028

Ghauch A, Tuqan A, Assi HA (2009) Antibiotic removal from water: elimination of amoxicillin and ampicillin by microscale and nanoscale iron particles. Environ Pollut 157(5):1626–1635. https://doi.org/10.1016/j.envpol.2008.12.024

Hajjaji W, Pullar RC, Labrincha JA, Rocha F (2016) Aqueous acid orange 7 dye removal by clay and red mud mixes. Appl Clay Sci 126:197–206. https://doi.org/10.1016/j.clay.2016.03.016

Kakavandi B, Esrafili A, Mohseni-Bandpi A, Jafari AJ, Kalantary RR (2014) Magnetic Fe3O4@C nanoparticles as adsorbents for removal of amoxicillin from aqueous solution. Water Sci Technol 69(1):147–155. https://doi.org/10.2166/wst.2013.568

Karimi E, Teixeira IF, Ribeiro LP, Gomez A, Lago RM, Penner G, Kycia SW, Schlaf M (2012) Ketonization and deoxygenation of alkanoic acids and conversion of levulinic acid to hydrocarbons using a red mud bauxite mining waste as the catalyst. Catal Today 190(1):73–88. https://doi.org/10.1016/j.cattod.2011.11.028

Karimi E, Teixeira IF, Gomez A, de Resende E, Gissane C, Leitch J, Jollet V, Aigner I, Berruti F, Briens C, Fransham P, Hoff B, Schrier N, Lago RM, Kycia SW, Heck R, Schlaf M (2014) Synergistic co-processing of an acidic hardwood derived pyrolysis bio-oil with alkaline red mud bauxite mining waste as a sacrificial upgrading catalyst. Appl Catal B Environ 145:187–196. https://doi.org/10.1016/j.apcatb.2013.02.007

Liang W, Couperthwaite SJ, Kaur G, Yan C, Johnstone DW, Millar GJ (2014) Effect of strong acids on red mud structural and fluoride adsorption properties. J Colloid Interface Sci 423:158–165. https://doi.org/10.1016/j.jcis.2014.02.019

Liu P, Zhang H, Feng Y, Shen C, Yang F (2015a) Influence of spacer on rejection of trace antibiotics in wastewater during forward osmosis process. Desalination 371:134–143. https://doi.org/10.1016/j.desal.2015.06.006

Liu P, Zhang H, Feng Y, Shen C, Yang F (2015b) Integrating electrochemical oxidation into forward osmosis process for removal of trace antibiotics in wastewater. J Hazard Mater 296:248–255. https://doi.org/10.1016/j.jhazmat.2015.04.048

Liu H, Hu Z, Liu H, Xie H, Lu S, Wang Q, Zhang J (2016a) Adsorption of amoxicillin by Mn-impregnated activated carbons: performance and mechanisms. RSC Adv 6(14):11454–11460. https://doi.org/10.1039/C5RA23256B

Liu W, Ma J, Shen C, Wen Y, Liu W (2016b) A pH-responsive and magnetically separable dynamic system for efficient removal of highly dilute antibiotics in water. Water Res 90:24–33. https://doi.org/10.1016/j.watres.2015.12.025

Liu Y, Naidu R, Ming H, Dharmarajan R, Du J (2016c) Effects of thermal treatments on the characterisation and utilisation of red mud with sawdust additive. Waste Manag Res 34(6):518–526. https://doi.org/10.1177/0734242X16634197

Mansouri H, Carmona RJ, Gomis-Berenguer A, Souissi-Najar S, Ouederni A, Ania CO (2015) Competitive adsorption of ibuprofen and amoxicillin mixtures from aqueous solution on activated carbons. J Colloid Interface Sci 449:252–260. https://doi.org/10.1016/j.jcis.2014.12.020

Marcelino RBP, Leão MMD, Lago RM, Amorim CC (2017) Multistage ozone and biological treatment system for real wastewater containing antibiotics. J Environ Manage 195:110–116. https://doi.org/10.1016/j.jenvman.2016.04.041

Mendonça FG, Gomes JPM, Tristão JC, Ardisson JD, Soares RR, Lago RM (2016) Novel reductive extraction process to convert the bio-oil aqueous acid fraction into fuels with the recovery of iron from wastes. Fuel 184:36–41. https://doi.org/10.1016/j.fuel.2016.06.099

Miller FA, Wilkins CH (1952) Infrared spectra and characteristic frequencies of inorganic ions. Anal Chem 24(8):1253–1294. https://doi.org/10.1021/ac60068a007

Moussavi G, Alahabadi A, Yaghmaeian K, Eskandari M (2013) Preparation, characterization and adsorption potential of the NH4Cl-induced activated carbon for the removal of amoxicillin antibiotic from water. Chem Eng J 217:119–128. https://doi.org/10.1016/j.cej.2012.11.069

Ni F, He J, Wang Y, Luan Z (2015) Preparation and characterization of a cost-effective red mud/polyaluminum chloride composite coagulant for enhanced phosphate removal from aqueous solutions. J Water Process Eng 6:158–165. https://doi.org/10.1016/j.jwpe.2015.04.003

Oliveira AAS, Teixeira IF, Ribeiro LP, Tristão JC, Dias A, Lago RM (2010) Magnetic amphiphilic composites based on carbon nanotubes and nanofibers grown on an inorganic matrix: effect on water-oil interfaces. J Braz Chem Soc 21:2184–2188

Oliveira AAS, Tristão JC, Ardisson JD, Dias A, Lago RM (2011) Production of nanostructured magnetic composites based on Fe0 nuclei coated with carbon nanofibers and nanotubes from red mud waste and ethanol. Appl Catal B Environ 105(1-2):163–170. https://doi.org/10.1016/j.apcatb.2011.04.007

Pascual J, Corpas FA, López-Beceiro J, Benítez-Guerrero M, Artiaga R (2009) Thermal characterization of a Spanish red mud. J Therm Anal Calorim 96(2):407–412. https://doi.org/10.1007/s10973-008-9230-9

Pereira MC, Oliveira LCA, Murad E (2012) Iron oxide catalysts: Fenton and Fenton-like reactions—a review. Clay Miner 47(3):285–302. https://doi.org/10.1180/claymin.2012.047.3.01

Pezoti O, Cazetta AL, Bedin KC, Souza LS, Martins AC, Silva TL, Santos Júnior OO, Visentainer JV, Almeida VC (2016) NaOH-activated carbon of high surface area produced from guava seeds as a high-efficiency adsorbent for amoxicillin removal: kinetic, isotherm and thermodynamic studies. Chem Eng J 288:778–788. https://doi.org/10.1016/j.cej.2015.12.042

Pinto PS, Medeiros TPV, Ardisson JD, Lago RM (2016) Role of [FeOx(OH)y] surface sites on the adsorption of β-lactamic antibiotics on Al2O3 supported Fe oxide. J Hazard Mater 317:327–334. https://doi.org/10.1016/j.jhazmat.2016.05.095

Pourakbar M, Moussavi G, Shekoohiyan S (2016) Homogenous VUV advanced oxidation process for enhanced degradation and mineralization of antibiotics in contaminated water. Ecotoxicol Environ Saf 125:72–77. https://doi.org/10.1016/j.ecoenv.2015.11.040

Pouretedal HR, Sadegh N (2014) Effective removal of amoxicillin, cephalexin, tetracycline and penicillin G from aqueous solutions using activated carbon nanoparticles prepared from vine wood. J Water Process Eng 1:64–73. https://doi.org/10.1016/j.jwpe.2014.03.006

Qin X, Liu F, Wang G, Li L, Wang Y, Weng L (2014) Modeling of levofloxacin adsorption to goethite and the competition with

phosphate. Chemosphere 111:283–290. https://doi.org/10.1016/j.chemosphere.2014.04.032

Rahimi S, Moattari RM, Rajabi L, Derakhshan AA, Keyhani M (2015) Iron oxide/hydroxide (α,γ-FeOOH) nanoparticles as high potential adsorbents for lead removal from polluted aquatic media. J Ind Eng Chem 23:33–43. https://doi.org/10.1016/j.jiec.2014.07.039

Saitoh T, Shibayama T (2016) Removal and degradation of β-lactam antibiotics in water using didodecyldimethylammonium bromide-modified montmorillonite organoclay. J Hazard Mater 317:677–685. https://doi.org/10.1016/j.jhazmat.2016.06.003

Santona L, Castaldi P, Melis P (2006) Evaluation of the interaction mechanisms between red muds and heavy metals. J Hazard Mater 136(2):324–329. https://doi.org/10.1016/j.jhazmat.2005.12.022

Sellaoui L, Lima EC, Dotto GL, Lamine AB (2017a) Adsorption of amoxicillin and paracetamol on modified activated carbons: equilibrium and positional entropy studies. J Mol Liq 234:375–381. https://doi.org/10.1016/j.molliq.2017.03.111

Sellaoui L, Mechi N, Lima ÉC, Dotto GL, Ben Lamine A (2017b) Adsorption of diclofenac and nimesulide on activated carbon: statistical physics modeling and effect of adsorbate size. J Phys Chem Solids 109:117–123. https://doi.org/10.1016/j.jpcs.2017.05.019

Smičiklas I, Smiljanić S, Perić-Grujić A, Šljivić-Ivanović M, Mitrić M, Antonović D (2014) Effect of acid treatment on red mud properties with implications on Ni(II) sorption and stability. Chem Eng J 242:27–35. https://doi.org/10.1016/j.cej.2013.12.079

Sutar H, Mishra SC, Sahoo SK, Chakraverty AP, Maharana HS (2014) Progress of red mud utilization: an overview. Am Chem Sci J 4:255–279

Teixeira APC, Tristão JC, Araujo MH, Oliveira LCA, Moura FCC, Ardisson JD, Amorim CC, Lago RM (2012) Iron: a versatile element to produce materials for environmental applications. J Braz Chem Soc 23:1579–1593

Teixeira IF, Medeiros TPV, Freitas PE, Rosmaninho MG, Ardisson JD, Lago RM (2014) Carbon deposition and oxidation using the waste red mud: a route to store, transport and use offshore gas lost in petroleum exploration. Fuel 124:7–13. https://doi.org/10.1016/j.fuel.2014.01.088

Tian G, Wang W, Zong L, Kang Y, Wang A (2016) A functionalized hybrid silicate adsorbent derived from naturally abundant low-grade palygorskite clay for highly efficient removal of hazardous antibiotics. Chem Eng J 293:376–385. https://doi.org/10.1016/j.cej.2016.02.035

Tor A, Cengeloglu Y (2006) Removal of congo red from aqueous solution by adsorption onto acid activated red mud. J Hazard Mater 138(2):409–415. https://doi.org/10.1016/j.jhazmat.2006.04.063

Tor A, Cengeloglu Y, Aydin ME, Ersoz M (2006) Removal of phenol from aqueous phase by using neutralized red mud. J Colloid Interface Sci 300(2):498–503. https://doi.org/10.1016/j.jcis.2006.04.054

Tor A, Cengeloglu Y, Ersoz M (2009) Increasing the phenol adsorption capacity of neutralized red mud by application of acid activation procedure. Desalination 242(1-3):19–28. https://doi.org/10.1016/j.desal.2008.03.028

Wang T, Pan X, Ben W, Wang J, Hou P, Qiang Z (2017) Adsorptive removal of antibiotics from water using magnetic ion exchange resin. J Environ Sci 52:111–117. https://doi.org/10.1016/j.jes.2016.03.017

Weng X, Sun Q, Lin S, Chen Z, Megharaj M, Naidu R (2014) Enhancement of catalytic degradation of amoxicillin in aqueous solution using clay supported bimetallic Fe/Ni nanoparticles. Chemosphere 103:80–85. https://doi.org/10.1016/j.chemosphere.2013.11.033

Ye J, Cong X, Zhang P, Hoffmann E, Zeng G, Liu Y, Fang W, Wu Y, Zhang H (2015) Interaction between phosphate and acid-activated neutralized red mud during adsorption process. Appl Surf Sci 356:128–134. https://doi.org/10.1016/j.apsusc.2015.08.053

Ye J, Cong X, Zhang P, Zeng G, Hoffmann E, Wu Y, Zhang H, Fang W (2016) Operational parameter impact and back propagation artificial neural network modeling for phosphate adsorption onto acid-activated neutralized red mud. J Mol Liq 216:35–41. https://doi.org/10.1016/j.molliq.2016.01.020

Yin J, Meng Z, Du M, Liu C, Song M, Wang H (2010) Pseudo-template molecularly imprinted polymer for selective screening of trace β-lactam antibiotics in river and tap water. J Chromatogr A 1217(33):5420–5426. https://doi.org/10.1016/j.chroma.2010.06.044

Yue Q, Zhao Y, Li Q, Li W, Gao B, Han S, Qi Y, Yu H (2010) Research on the characteristics of red mud granular adsorbents (RMGA) for phosphate removal. J Hazard Mater 176(1-3):741–748. https://doi.org/10.1016/j.jhazmat.2009.11.098

Zboril R, Mashlan M, Petridis D (2002) Iron(III) oxides from thermal processes synthesis, structural and magnetic properties, Mössbauer spectroscopy characterization, and applications. Chem Mater 14(3):969–982. https://doi.org/10.1021/cm0111074